Magnetization study of γ-$Fe_{80-x}Ni_xCr_{20}$ ($14 \leqslant x \leqslant 30$) alloys to 20 T

T. K. Nath and N. Sudhakar
Department of Physics, Indian Institute of Technology, Kanpur 208016, India

E. J. McNiff
Francis Bitter National Magnet Laboratory, Massachusetts Institute of Technology, Cambridge, Massachusetts 02139

A. K. Majumdar
Department of Physics, Indian Institute of Technology, Kanpur 208016, India

(Received 26 February 1996; revised manuscript received 6 December 1996)

Very-high-field (0–20 T) dc-magnetization measurements $M(H)$ and $M(T)$ between 4.2–60 K and 19–700 K, respectively, have been carried out on substitutionally disordered γ-$Fe_{80-x}Ni_xCr_{20}$ ($14 \leqslant x \leqslant 30$), austenitic stainless steel alloys having a wide variety of exotic magnetic phases. Distinct functional relationships $M(H)$ have been found in different magnetic phases below their respective transition temperatures. In a ferromagnetic (FM) alloy with $x=30$, contributions from long-wavelength spin-wave and Stoner single-particle excitations have been found in the temperature-dependent demagnetization process. In the light of the Rhodes-Wohlfarth criterion, this alloy is found to be a weak-itinerant FM. For the alloys with $x=26$ and 23 (mixed or reentrant phase) the coexistence of long-range FM ordering along with spin-glass (SG) freezing has been established supporting the Gabay-Toulouse model. For $x=21$ and 19 (SG), the field-dependent magnetization (after scaling) falls on a single universal curve, which implies the same kind of response dynamics of the frozen spins. For an antiferromagnetic (AFM) alloy with $x=14$, a spin-flop transition has been observed at 1 T due to the canting of the AFM spins in the strong external magnetic field. The long-range AFM structure of this alloy is found to be of type 1. [S0163-1829(97)02817-8]

I. INTRODUCTION

The magnetism of $3d$ transition metal alloys is still of great interest because no unique theory has emerged which could explain by and large all experimental results. None of the two extreme models, namely, the Heisenberg theory of localized spins and the Stoner's itinerant electron model, are successful in that sense. A lot of effort[1,2] has been put into finding a unified theoretical model making a compromise between these two extreme ones.

In recent years, there has been a lot of theoretical effort to understand the nature of magnetism and the magnetic band structure of $3d$ transition metals and their binary alloys. A number of approaches and techniques has been employed, namely, the local density approximation (LDA), coherent potential approximation (CPA), and cluster coherent potential approximation (CCPA) with Koringa-Kohn-Rostoker (KKR) formalism, local-spin-density calculation (LSD), linear muffin-tin orbital (LMTO), fixed spin moment (FSM), finite-temperature theory of local environment effect (LEE) on Fe-Co binary alloys,[3] density functional theory (DFT),[4] etc. The local density calculation, taking into account all effects of electron exchange and correlation, correctly describes the itinerant magnetism of $3d$ transition metals and alloys with nonintegral values of spins. Electronic and magnetic band structure calculations for itinerant systems have become very promising.

No real system behaves exactly like either of the above two models. Magnetism in $3d$ transition metals and alloys is itinerant, but it does have some aspects of localization.[5] The orbital moment does not vanish completely in these systems. It has been found from different experiments[6] that not all $3d$-$3d$ alloys follow the Slater-Pauling curve (e.g., Ni-Cr, Ni-V, etc., alloys) which is mainly because of the formation of virtual bound states above the Fermi level as suggested by Friedel.[7] These are due to the presence of strong perturbations around the impurities (e.g., Cr or V in Ni host), resulting in a splitting up of an impurity state above the Fermi level. Neutron scattering experiments in a series of Ni-based alloys[8] have demonstrated the correctness of Friedel's prediction of strong magnetic disturbances associated with impurities of transition metals. Low and Collins[8] found that around Fe and Mn impurities in a Ni matrix the moment disturbances are effectively confined to the solute atom site, whereas V or Cr impurities markedly reduce the magnetic moment on neighboring Ni atoms.

In magnetic materials (either crystalline or amorphous), a random mixture of ferromagnetic (FM) and antiferromagnetic (AFM) bonds, having strongly competing interactions between them (in the Heisenberg picture), may lead to a diversity of magnetic structures at low temperatures. There could be a critical concentration range where FM and AFM exchange contributions to the free energy are equal. The ground state in this concentration range may be imagined as a spin-glass (SG) state with short-range FM and AFM orders. In recent years attempts have been made to go beyond the mean-field approximation and develop a theory of spin glass with a finite range of interaction.[9] Far away from critical concentration a long-range (FM and AFM) magnetic ordering generally sets in (e.g., Fe-Ni, Ni-Mn, Fe-Ni-Mn, Fe-Cr, Au-Cr, etc.).

In the vicinity of a multicritical point, there is a subtle

interplay between the long-range magnetic ordering and the randomness of the SG state. There could also be a particular regime near the critical concentration which may exhibit double magnetic transitions, one at a higher temperature T_c (PM→FM) and another (FM→mixed FM and SG) at a lower temperature T_f. These are called mixed or reentrant phase alloys (e.g., Au-Fe, Fe-Cr, Ni-Mn, Al-Fe, Fe-Ni-Mn, Cr-Fe, etc.). A reentrant transition from an AFM state has been observed in $FeMgCl_2$ and Mn-rich CuMn binary alloys.[10,11] The existence of sequential (double) magnetic phase transitions in a FM with a substantial degree of exchange bond disorder continues to be a topic of considerable interest.

During the last decade, reentrant SG transitions have been investigated extensively both theoretically[12–14] and experimentally[15–20] by means of different techniques including not only bulk magnetic measurements but also other methods probing the magnetic structure on a microscopic scale (e.g., small-angle neutron scattering and neutron depolarization studies,[21,22] Mössbauer study,[23,24] electron spin resonance, muon spin resonance, etc.). However, the exact nature of the reentrant transition is still unclear and highly controversial because of several debatable questions like the following: What is the nature of magnetization in the so-called FM phase ($T_f \leqslant T \leqslant T_c$) for this kind of alloy? What happens to it in the reentrant or mixed phase ($T < T_f$)? Does long-range FM ordering coexist with SG ordering or is it a pure SG phase due to random freezing of spins at a temperature $T < T_f$? What are the physical origins of the field and temperature dependence of the bulk magnetization $M(T,H)$ near and below T_f?

In the light of the mean-field models of Heisenberg ($3d$ vector spins) systems, Gabay and Toulouse[12] (GT) theoretically predicted the most plausible nature of magnetic transitions in mixed phase alloys. According to them a sequence of three kinds of magnetic transitions is possible with decreasing temperature which are (i) PM→FM followed by (ii) a transition (crossing GT line) to a mixed phase where the FM state coexists with transverse SG ordering (say, in the x-y plane) because of the random freezing of spins and a longitudinal long-range FM ordering with spontaneous magnetization in the direction of broken symmetry (say, the z axis), (iii) a crossover from weak to strong irreversibility [crossing the Almeida-Thouless line (AT)]. Magnetic phase diagrams of such systems [$(Pd_{1-y}Fe_y)_{1-x}Mn_x$,[25] AuFe,[15] Fe-Cr, Ni-Mn, $EuSr_{1-x}S_x$, Fe-Ni-Mn,[16] etc.] exhibit features which bear resemblance, at least superficially, to the prediction of the vector–mean-field model as predicted by Gabay and Toulouse.

However, no rigorous experimentally accessible criterion is currently available for assessing the genuine cooperative nature of the mixed phase transitions. Moreover, recently there have been some reports on the intermetallic compounds $CeFe_2$,[26,27] UCu_2Ge_2,[28] etc., which reveal that all these systems undergo transitions from a long-range FM state at higher temperature to an AFM state at lower temperature via a canted phase. They show almost the same features as the so-called reentrant or mixed phase systems. The interpretation of such types of magnetic phase transitions is sought within the model put forward by Morya and Usami[29] for itinerant system of electrons with strong correlation.

It is known that γ-FeNiCr alloys have competing exchange interactions[30,31] because of which the local spin orientation is expected to depend on its environment. The effective exchange interaction can be positive, negative, or nearly zero. In the Heisenberg local moment picture, the behavior of the whole sample will be governed by the concentration, distribution, and strength of the six different possible exchange interactions J_{ij} between the different magnetic atoms. As a result, a number of exotic magnetic phases are realized at low temperatures. In the present investigation we have chosen a particular series of γ-$Fe_{80-x}Ni_xCr_{20}$ ($14 \leqslant x \leqslant 30$) substitutionally disordered alloys of type-304 polycrystalline austenitic stainless steel. These isostructural (fcc structure) alloys are the closest realization of γ-Fe, the nature of the ground state of which was highly controversial but later on confirmed to be AFM.[32,33] In γ-Fe two other issues[34] related to itinerant electron magnetism are also important: (i) the nature of magnetic interaction and (ii) the localizaton of magnetic moments.

Although γ-Fe is unstable at room temperature, the fcc allotrope could be obtained by alloying with Ni and the resulting structure stabilized by the addition of Cr, Mn, V, or Cu.[6,35] These austenitic stainless steels have many industrial applications. They are highly corrosion resistant because of the formation of a thin impervious layer of Cr_2O_3.[35] They are also nontoxic and nonmagnetic and can be used as cryogenic materials. They are also used for sophisticated pharmaceutical equipment and as creep-resistive and high-resistance materials.[35] The magnetic phase diagram[30,31] had been established in γ-$Fe_{80-x}Ni_xCr_{20}$ ($14 \leqslant x \leqslant 30$) through dc-magnetization,[30] magnetic neutron scattering,[36,37] and ac-susceptibility measurements. Due to strong competing exchange interactions between different kinds of $3d$ transition metal magnetic ions, this system of alloys undergoes a compositional phase transition from long-range AFM ($x = 10$–14) to SG (17–21), to mixed FM and SG (23–26) or reentrant phase, and finally to long-range FM (30) order within the same crystallographic phase. To our knowledge, so far there is no electronic or magnetic band structure calculation in this series of ternary magnetic alloys having such wide varieties of magnetic phases. The present investigation might lead to band structure calculations in this kind of magnetic system.

We had reported earlier[38] that the magnetoresistance (MR) of all these alloys is negative until as high as 50 K in the field range of 0 to 2 T. A striking correlation between the magnetization and the MR was observed only in the SG alloys ($x = 19,21$) with $\Delta\rho/\rho \propto M^{2.5}$. The isotropic nature of the MR as well as the thermomagnetic history effect of the field-cooled (FC) magnetization[38,30] confirmed the freezing of spins at the lowest temperatures in the alloys which have SG (19,21) and mixed (23,26) phases at those temperatures. The role of the different magnetic phases (due to short- and long-range spin orderings) on electronic transport has been throughly investigated using ρ(T) measurements[39,40] in this system of alloys. In Table I, we have listed the values of their magnetic transition temperatures (T_c, T_f, and T_N). It was found from low- and intermediate-field magnetization[38,30] studies that the alloy with $x = 30$ behaves like a distorted or inhomogeneous FM unlike the conventional FM. Isothermal magnetization curves, in the PM state of each alloy, have

TABLE I. Fit of the isothermal M-H curves of $Fe_{80-x}Ni_xCr_{20}$ alloys to several distinct fit functions until 20 T: compositions (x), fit functions, fit parameters (M_0, M_1, and n), field range, temperature, and the values of χ^2.

x (Ni conc.)	Fit function	M_0 (emu/g)	M_1 (emu/gT^n)	n	Field range (T)	Temperature (K)	χ^2 [a] (10^{-6})
30	$M=M_0+M_1H^n$	32.0	5.4	0.35	1 – 20	4.2	1.2
(T_c=130 K)							
26	$M=M_0+M_1H^n$	18.7	7.0	0.38	2 – 20	4.2	1.8
(T_c,T_f		19.3	6.3	0.39	2 – 20	8.1	1.5
= 60, 7 K)		19.1	5.2	0.42	2 – 20	20.7	0.88
		11.2	6.9	0.40	2 – 20	59.8	0.72
19	$M=M_1H^n$		10.0	0.34	1 – 20	4.2	0.3
(T_f=12 K)			9.9	0.34	1 – 20	8.1	0.16
			9.1	0.36	1 – 20	20.2	0.17
14	$M=M_1H^n$		2.3	1.04	0 – 1.5	4.2	0.2
(T_N=26 K)			3.6	0.53	5 – 20	4.2	0.4
			3.5	0.54	5 – 20	11.2	1.9
			3.3	0.56	5 – 20	20.1	1.5
			2.7	0.60	5 – 20	35.3	2.5
			1.8	0.71	5 – 20	59.8	4.9

[a] $\chi^2=(1/N)\Sigma_{i=1}^{N}[Y^i_{\text{expt}}-Y^i_{\text{fit}}]^2/(Y^i_{\text{expt}})^2$.

strong curvatures even at temperatures much higher than their respective transition temperatures. Also their M-H curves did not show any tendency of saturation even until 6 T and down to 4.2 K.[30]

The motivation behind the present investigation is to seek answers to many questions; e.g., what are the very high-field magnetic responses (χ_{HF}) of these wide varieties of magnetic phases (FM, mixed, SG, and AFM) which are very close to the critical concentration and in which very strong competing exchange interactions exist? Also, is it possible to find in them distinct functional relationships between magnetization and magnetic field at high fields ?

II. EXPERIMENTAL DETAILS

The alloys $Fe_{80-x}Ni_xCr_{20}$ with $x=14$, 19, 21, 23, 26, and 30 were prepared[30] by induction melting in an argon atmosphere from metals of at least 99.99% purity. The samples were cut into rods of uniform dimensions so as to have known demagnetization factors needed for magnetization measurements. Then they were annealed at 1050 °C for 30 h in an argon atmosphere and quenched rapidly to room temperature in brine. All the samples were characterized by x-ray diffraction (XRD) to investigate the possible presence of any second phase (say, of bcc structure) apart from the fcc γ phase. The diffraction patterns revealed that all the alloys were single phase fcc similar to that of austenitic γ-Fe, with lattice parameter $a=(3.58\pm0.01)$ Å. The nominal compositions were verified through scanning electron microscope (SEM) and energy dispersive x-ray (EDAX) analysis. The analyzed compositions are found to be within 0.5% of the nominal ones for Ni and Cr.

The dc-magnetization (M-H) measurements were carried out using a computer-contolled vibrating sample magnetometer (VSM) (model PAR, FM-1) adapted with a water-cooled Bitter coil magnet (2-T type) of 52.5 mm bore at FBNML, MIT. All the M-H measurements were done between 4.2 and 60 K and up to magnetic fields as high as 20 T using a 10-MW power supply.[41] The data acquisition was done through a PC/AT in both continuous scanning increasing and decreasing field modes. The temperature of the sample was measured by a calibrated carbon resistor, glued to the vibrating rod between the heater and the sample. However, the temperature was controlled by a similarly mounted glass-ceramic capacitance sensor and matching electronics.

The low-field dc-magnetization measurements were more accurate and were carried out between 19 and 300 K in magnetic fields up to 1.6 T using a VSM (model PAR, 155), a Varian 15″ electromagnet and a closed-cycle helium refrigerator (CTI). A 100-Ω precalibrated platinum resistance thermometer, mounted very close to the sample, was used to monitor the temperature.

A high-temperature oven assembly was used for the dc-magnetization measurements in the temperature range 300–700 K. A special high-temperature vibrating rod attachment, which consists of a fused quartz extension with high-purity boron-nitride guides and sample holder cup, is used for this purpose. Inert helium gas was used at the sample zone because its high thermal conductivity provided a good thermal contact between the sample and the hot wall surrounding it.

Both VSM's were calibrated with a standard Ni sample. The absolute accuracy in dc-magnetization measurements was better than 1 part in 2500. The stability of temperature during the measurements was within ± 100 mK below 60 K.

III. RESULTS AND DISCUSSION

A. General features of the high-field M-H curves between 4.2 and 60 K and low-field M-T curves between 19 and 700 K

In Fig. 1 we show the high-field dc-magnetization (M-H) curves of substitutionally disordered γ-$Fe_{80-x}Ni_xCr_{20}$

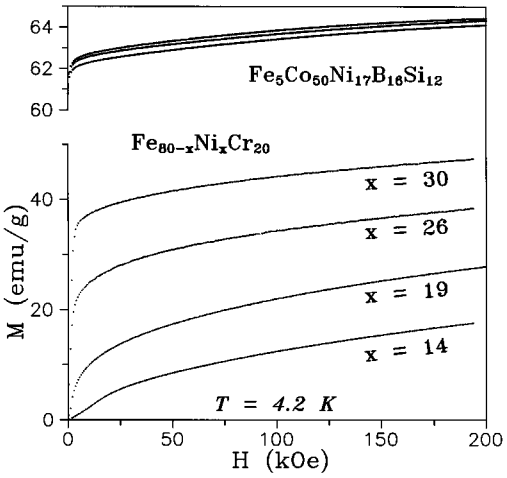

FIG. 1. Experimental $M(H)$ plots of $Fe_{80-x}Ni_xCr_{20}$ ($x=14$, 19, 26, and 30) austenitic stainless steel alloys in the magnetic field range of 0–20 T at 4.2 K. The topmost three curves are the *M-H* plots of $Fe_5Co_{50}Ni_{17}B_{16}Si_{12}$ amorphous ferromagnetic metallic glass at 4.2, 8.1, and 20.1 K.

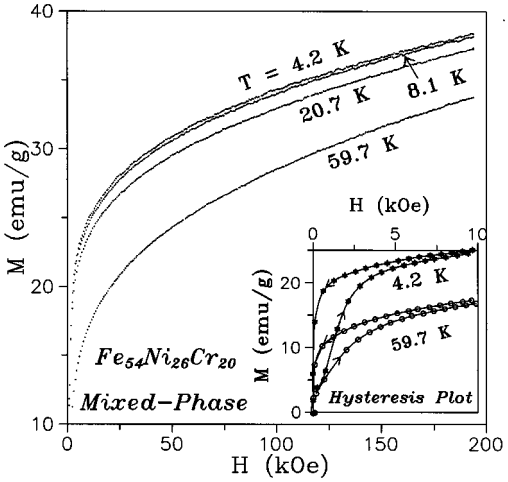

FIG. 2. *M-H* isotherms of the mixed phase alloy $Fe_{54}Ni_{26}Cr_{20}$ at 4.2, 8.1, 20.7, and 59.7 K in the field range of 0–20 T. The inset shows its hysteresis plot which is a measure of the field-induced anisotropy energy at 4.2 and 59.7 K in the low-field range of 0–1 T.

alloys with $x=14$, 19, 26, and 30, up to a field of 20 T at 4.2 K, which is much below their respective transition temperatures (T_c, T_f, and T_N given in Table I). We also show the *M-H* plots of the amorphous FM metallic glass $Fe_5Co_{50}Ni_{17}B_{16}Si_{12}$ (Ref. 42), at 4.2, 8, and 20 K for comparison. From the high-field *M-H* curves at 4.2 K and also at several higher temperatures (not shown) the following observations are made.

(1) The magnetization of the alloy with $x=30$ approaches a saturation value much faster than all the other alloys of the series (Fig. 1). However, even at a field as high as 20 T there is sufficient curvature even at 4.2 K and the magnetization is yet to attain saturation. The high-field susceptibility ($\chi_{HF} \equiv dM/dH|_{H=19\ T} \approx 0.3\times10^{-4}$ cm^3/g) is fairly large as compared to that of $Fe_5Co_{50}Ni_{17}B_{16}Si_{12}$ ($\approx 0.8\times10^{-6}$ cm^3/g), a conventional FM.

(2) In the case of the alloy with $x=26$ which has a mixed phase ordering at 4.2 K, there is a large induced moment above the technical saturation. The magnetization is still increasing (very hard to saturate) even at 20 T with $\chi_{HF} \approx 0.45\times10^{-4}$ cm^3/g. This value is also very large compared to that of a conventional FM. The magnetization curves even below 20 K ($\approx T_c/3$) show no tendency to converge towards the 4.2 K curve (Fig. 2) even at such high fields. This behavior is in contrast with the case of a standard FM in which a strong external field suppresses the thermal spin fluctuations, thereby recovering the moment. In the inset of Fig. 2 we show the low-field hysteresis curves of this alloy at 4.2 and 59.7 K. The area enclosed by the increasing and decreasing magnetization curves corresponds to the field-induced anisotropy energy which decreases with temperature (inset of Fig. 2) and vanishes at higher temperatures. This kind of high-field *M-H* curve has a strong resemblance to those of many crystalline and amorphous materials which have mixed phases at low temperatures [e.g., AuFe (with 14–18 at. % Fe),[43] FeZr,[44] etc., at the critical concentration regime].

(3) The high-field *M-H* curve for the alloy with $x=19$ (SG) is much steeper even at the lowest temperature of 4.2 K which is below the spin-freezing temperature. The competing random exchange interactions between the FM and the AFM bonds result in a very large value of the high-field susceptibility χ_{HF} ($\approx 0.6\times10^{-4}$ cm^3/g) at 19 T.

(4) The *M-H* curve of the alloy with $x=14$, which has an AFM ordering below $T_N = 26$ K, however, shows a striking change of slope at around 1 T at 4.2 K (Figs. 1 and 3). This abrupt change of slope is more pronounced in the dM/dH vs H plot (Fig. 3) which shows a peak at 1 T. However, it vanishes completely at 35.3 K (not shown). This sudden change of slope may be attributed to a *spin-flop* transition because of the canting of the AFM spins in this alloy.

(5) No abrupt change in the behavior of the *M-H* curves is observed in the FM→AFM critical concentration range.

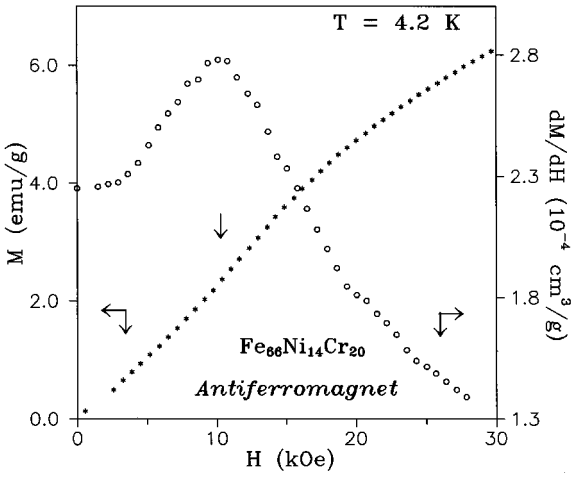

FIG. 3. *M-H* and dM/dH vs H plots of the AFM alloy $Fe_{66}Ni_{14}Cr_{20}$ at 4.2 K. The *M-H* plot shows a striking change of slope around 1 T (shown by an arrow) where dM/dH shows a peak. This has been attributed to a *spin-flop* transition at this field.

TABLE II. Concentration dependence of different fit parameters (M_s, a, and b) of the law of approach to saturation [Eq. (2)], the values of χ^2, temperature, and field range for several isothermal M-H curves of $Fe_{80-x}Ni_xCr_{20}$ alloys.

x (Ni conc.)	Temperature (K)	Field range (T)	M_s (emu/g)	a (emu T/g)	b (emu/gT)	χ^2 (10^{-7})
30	4.2	3 – 20	42.6	13.00	0.30	7.4
26	4.2	5 – 20	32.6	17.64	0.40	0.18
	8.1	5 – 20	32.9	22.20	0.35	0.11
	20.7	5 – 20	31.9	23.78	0.38	7.9
	59.7	5 – 20	25.9	20.57	0.46	9.6
19	4.2	5 – 20	19.8	24.60	0.52	5.6
	8.1	5 – 20	19.6	24.40	0.47	4.8
	20.2	5 – 20	18.7	24.20	0.48	4.4
14	4.2	5 – 20	9.3	16.60	0.45	0.16
	11.2	5 – 20	9.3	17.62	0.47	0.21
	20.1	5 – 20	9.0	17.63	0.48	0.23
	35.3	5 – 20	8.0	17.26	0.48	0.28
	59.8	5 – 20	5.8	14.64	0.52	0.30

The M-H curves of all the alloys have sufficient curvatures even at temperatures much higher than their respective transition temperatures. This may be due to the effect of clustering, short-range ordering, or local frozen spin moments in the PM state.

We have made an attempt to fit all the high-field M-H curves of this series of alloys to some empirical relations. Nonlinear log M vs log H plots reveal that for the alloys with $x=30$ and 26, M is not solely dependent on a single term in H. However, the alloy with $x=19$ shows a perfectly linear log-log plot, implying $M \propto H^n$. The alloy with $x=14$ also shows a linear log-log plot with two distinct slopes below and above the *spin-flop* transition. So we have taken a general empirical relation

$$M = M_0 + M_1 H^n \tag{1}$$

to fit all the M-H curves employing a nonlinear least-squares fitting program along with a EO4FDF NAG subroutine. We have kept M_0, M_1, and n as adjustable parameters to fit the $M(H)$ data. In the case of alloys with $x=19$ and 14, the values of M_0 are negligibly small and have been neglected. Table I gives the fitting parameters for all the alloys at several temperatures. From Table I, the following inferences can be drawn.

In the case of the alloys with $x=30$ and 26, the inclusion of the additional constant term M_0 makes the quality of fit much better ($\chi^2 \sim 10^{-6}$ is comparable to the experimental accuracy). M_0 is maximum for the alloy with $x=30$ at 4.2 K. In the case of the alloy with $x=26$, because of the freezing of the X-Y components of spins (according to the GT model) below 7 K, the spontaneous moment (M_0) at 4.2 K has gone down slightly as compared to that at 8.1 K. This kind of observation could also be made from the M-T plots.[30] The decrease in M_0, above 8.1 K, due to an enhancement of thermal spin fluctuations as well as spin-wave excitations, is quite reasonable. In the case of the alloys with $x=14$ (AFM) and 19 (SG), M_0 is negligibly small. The M_0 term has been attributed physically to the spontaneous moments of these alloys. Its values are found to be consistent with their magnetic phases.

In the case of the alloy with $x=30$, the value of the exponent of H is $n \approx 1/3$ at 4.2 K whereas for the alloy with $x=26$ it is $\approx 3/7$. Considering the infinite-range Ising interaction, Toulouse[45] had suggested a model for mixed phase systems where $M \sim H^{3/7}$, in good agreement with our observation. For $x=19$, $n \approx 1/3$. In the case of the alloy with $x=14$, the exponents are $n \approx 1$ and 1/2 in lower- and higher-field ranges, respectively. This implies that in the AFM state, below the *spin-flop* transition, M has a linear dependence on H whereas above it $M \propto \sqrt{H}$.

As discussed earlier, in the γ-$Fe_{80-x}Ni_xCr_{20}$ ($14 \leqslant x \leqslant 30$) alloys, because of the presence of strongly competing exchange interactions between different pairs of magnetic atoms,[30,37] critical concentration is attained for this particular range of stoichiometry. As a result it hinders the rotation of the magnetic spins and so a saturation of the magnetization is hard to achieve (Figs. 1 and 2) even at 20 T and 4.2 K. However, one cannot rule out the possibility of the formation of either short-range clustering or clustering of local spin freezing as well as the existence of local anisotropy and intrinsic fluctuation of the material parameters as in the case of AuFe,[46] FeZr,[47] etc.

We have also analyzed the data in terms of the law of approach to saturation, given empirically by

$$M = M_s - \frac{a}{H} + bH, \tag{2}$$

where M_s is the saturation magnetization and the a/H term is attributed to the intrinsic fluctuation of the material parameter, viz., presence of nonmagnetic voids, inclusions, and microstress. All our samples are cold rolled and after the final annealing process, to retain the γ phase, they had to be quenched from 1050 °C to room temperature. This has caused mechanical hardening of the samples as a result of the microstress developed. The last term, bH, corresponds to the

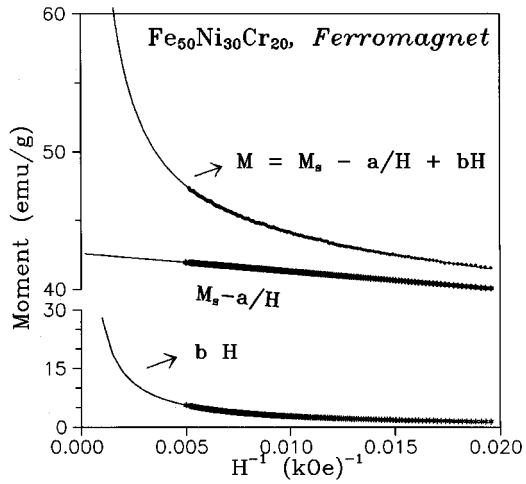

FIG. 4. M vs H^{-1} plot of $Fe_{50}Ni_{30}Cr_{20}$ (FM) alloy. The solid line of the topmost curve is the extrapolation of the fit to Eq. (2) in the very-high-field range. The other two curves are the resolved contributions.

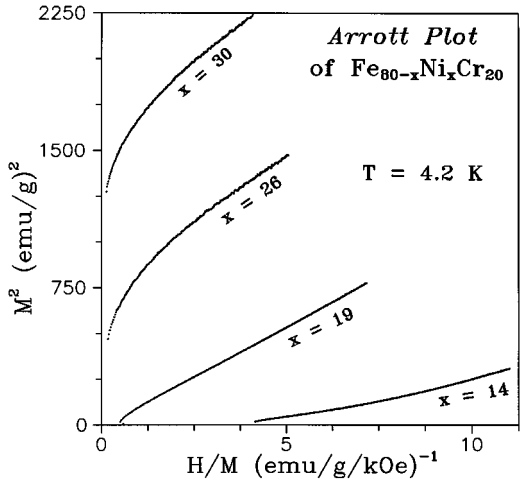

FIG. 5. Arrott plots (M^2 vs H/M) of crystalline $Fe_{80-x}Ni_xCr_{20}$ (x = 14, 19, 26, and 30) alloys with wide varieties of magnetic phases at 4.2 K. The curvature changes (convex to concave) while passing through the critical concentration region.

high-field susceptibility χ_{HF} ($\approx \delta M/\delta H|_{H\to\infty} \approx b$). We have fitted all the M-H data to Eq. (2) keeping M_s, a, and b as adjustable parameters. In Table II we have summarized the values of the parameters along with the values of χ^2. From Table II a number of observations can be made. The quality of fit is good, and the $\chi^2 \approx 10^{-7}$ is comparable to the experimental accuracy. The saturation magnetization (M_s) increases with Ni concentration (x) at a particular temperature whereas it decreases with temperature for the same x. The constant a and the high-field susceptibility b ($\approx \chi_{\mathrm{HF}}$) both increase with x and attain maxima at around $x=19$ (critcal concentration range) and then they decrease with further increase of x. This shows that for the alloys with long-range FM ($x=30$) and AFM ($x=14$) orderings, the high-field susceptibility χ_{HF} is much smaller than those of the alloys which have SG and mixed phase orderings at low temperatures.

In Fig. 4 we show the individual contributions of $M_s - a/H$ and bH terms along with the total M plotted against $1/H$ for $x=30$ at 4.2 K. The figure shows how the magnetization approaches saturation in the high-field region $[(1/H)\to 0]$. It is also clear from this analysis that even the 20-T field is not sufficient to align all the spins to reach saturation. The extrapolation with Eq. (2) (as shown in Fig. 4) suggests that it may require a field as high as 100 T to align all the spins with a maximum value of $M \approx 70$ emu/gm.

Figure 5 is the Arrott-Belov-Kouvel (ABK) plot (using mean-field values of the critical exponents $\beta=0.5$ and $\gamma=1$) for $x=30$, 26, 19, and 14 alloys at 4.2 K. This is a very important plot to confirm the presence of any FM phase from the finite value of the spontaneous moment in the absence of any internal magnetic field. In the high-field linear regions, we have fitted straight lines and estimated the spontaneous moments (M_0) from the positive intercepts. The alloy with $x=30$ (FM) has a very high value of spontaneous moment as compared to those of the others. For the alloy with $x=26$ (mixed) we confirm the persistence of the FM ordering even below the SG freezing temperature from the positive intercept on the M^2 axis. Had it been in a pure SG phase, it would not have shown any positive intercept. In our earlier work[38] we had confirmed the coexistence of FM and SG orderings in the alloy with $x=23$ (mixed phase). In the case of the alloy with $x=19$ (SG), the negative intercept on the M^2 axis even at 4.2 K rules out any possible FM ordering. For $x=14$ (AFM), the ABK plot has a strong concave curvature in the low-field region as opposed to the convex ones for the FM and mixed phase alloys.

In the alloys with higher Ni concentraion, the FM states are either weak or inhomogeneous having very high values of χ_{HF}. The spontaneous moments (M_0) from the intercepts of the ABK plot at 4.2 K are (0.39, 0.27, 0.13) $\mu_B/\langle \mathrm{atom} \rangle$, respectively, for $x=30$, 26, 23. These values strongly deviate from the Slater-Pauling curve for the $3d$ transition metals and alloys. This may be understood in the light of Friedel theory of the formation of VBS and the split-band model.

The Arrott plots for $x=26$ at several higher temperatures (Fig. 6) also show a change of curvature from concave to

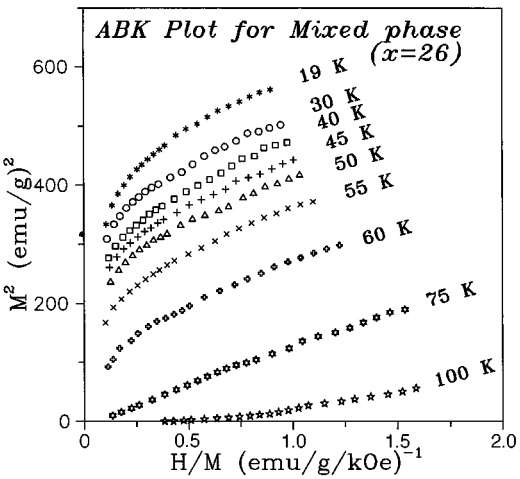

FIG. 6. Arrott-Belov-Kouvel (ABK) plots at various temperatures in the low-field range for the mixed phase alloy $Fe_{54}Ni_{26}Cr_{20}$ confirming the presence of the FM ordering.

convex while passing through the Curie temperature from the high-temperature side. So there exists a close analogy between what happens for a fixed concentration when the temperature is changed and the case where the temperature is fixed and the concentration is varied. There could be several reasons for the deviations from linearity of the ABK plots for all the alloys in the low-field range: (1) An inhomogeneous character of magnetization may be associated with such deviations (e.g., amorphous Fe-Ni alloys near the critical concentration[48]). (2) According to Shtrikman and Wohlfarth,[49] for heterogeneous weak itinerant magnetic alloys, the deviation from linearity is attributed to spatial inhomogenities of the magnetization due to fluctuations in concentration. (3) For a homogeneous magnetic system the Arrott plots give straight lines in the case of weak ferromagnetic materials except at the lowest fields where domain rotations occur.[50] The ABK plots for a SG or a mictomagnetic phase at high enough fields and temperatures as well as for a mixed phase, where FM and cluster glass or SG coexist, should be rather curved.[48] Some experimental evidence for FeCr, FeMnPC, etc., alloys[51,48] supports this kind of behavior.

Based on the Stoner model, Edwards, Wohlfarth, and Mathon had applied the Landau-Ginzberg theory of the second-order phase trasition to FM metals and alloys whose magnetization M is low compared to that for a complete alignment of spins and obtained

$$H/M(H,T,c)=A(T,c)+B(T,c)M^2(H,T,c), \qquad (3)$$

where A and B are the Landau coefficients and c is the concentration. We observe that the value of B^{-1} (120, 138, and 162 [(emu/g)^3/T], respectively, for $x=23$, 26, and 30 after fitting the M-H data to Eq. (3) in the high-field linear regime (Fig. 5)) gradually increases with the increase in Ni concentration (x). Comparing the concentration dependence of the specific heat[52] which also increases with x, one can qualitatively argue that because of the increase of the density of states at Fermi level $[N(E_F)]$ with x, the value of B^{-1} is enhanced. This result supports the Edwards and Wohlfarth's theoretical prediction.[50] We have also found (not shown) that for the alloys with $x=30$, 26, and 23, $T_c^2 \sim x$ (Ni concentration), $M^2(0,0,x)\sim x$ and $\chi_0^{-1}\sim x \sim |c-c_{\rm crit}|$. Plots of these quantities are called Mathon plots, where $c_{\rm crit}$ is the critical concentration for weak itinerant ferromagnetism.[53] This provides us a better understanding of the weak itinerant type of FM ordering which exists in these disordered $3d$ transition metal alloys.

As mentioned earlier we have carried out dc magnetization measurements between 20 and 700 K in a constant dc field of 0.2 T, to examine whether in the pure paramagnetic regime they follow the Curie-Weiss law. In Figs. 7 and 8 we show typical $1/\chi$ vs T plots for the alloys with $x=19$, 30, and 14. We find that (Fig. 7) all the alloys obey the Curie-Weiss (CW) law in the high-temperature range. The deviation from the CW law starts at temperatures (T_d) much higher than their respective transition temperatures. This kind of behavior also shows up in the nonlinearity of the M-H curves (CW law gives $M \propto H$ at constant temperature) even much above their respective transition temperatures. This may be due to the persistence of some short-range ordering. From the high-temperature ($T>T_d$) data we have

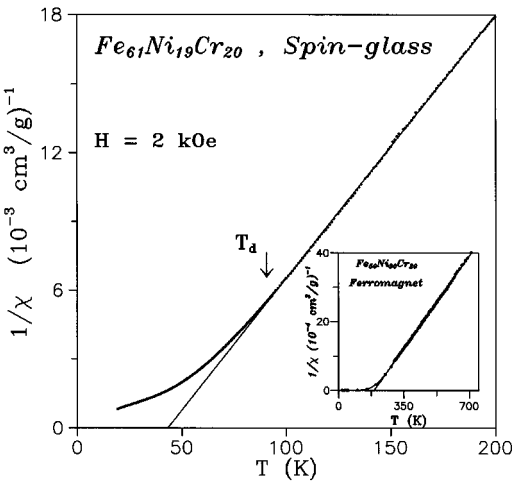

FIG. 7. Reciprocal susceptibility ($1/\chi$) vs temperature (T) for $Fe_{61}Ni_{19}Cr_{20}$ (SG) alloy at 0.2 T. The arrow shows the onset ($T_d \gg T_f$) of the deviation from the Curie-Weiss behavior. The inset shows the same plot for $Fe_{50}Ni_{30}Cr_{20}$ (FM) alloy. The solid lines are the fits to Curie-Weiss law.

estimated the Curie constant (C) and the paramagnetic Curie temperature (Θ) for each alloy from the slopes and intercepts of the linear fits. Table III lists quantities like C, $P_{\rm eff}$, Θ, etc., where $P_{\rm eff}$ is the effective Bohr magneton number given by

$$P_{\rm eff}=g[J(J+1)]^{1/2}=\left\{(3k_B)\Big/\left[N_x\mu_B^2\frac{d}{dT}\left(\frac{1}{\chi}\right)\right]\right\}^{1/2}. \qquad (4)$$

Here N_x is the average number of the three kinds of atoms (Fe, Ni, and Cr) per gram, g the Landé g factor, J the total angular momentum, k_B the Boltzmann constant, and μ_B the Bohr magneton. Θ is found to be increasing roughly linearly with x while the variation of $P_{\rm eff}$ with x is rather small. Figure 8 clearly shows the AFM transition for the alloy with $x=14$ where a peak in $M(T)$ occurs at $T_N=(26\pm1)$ K.

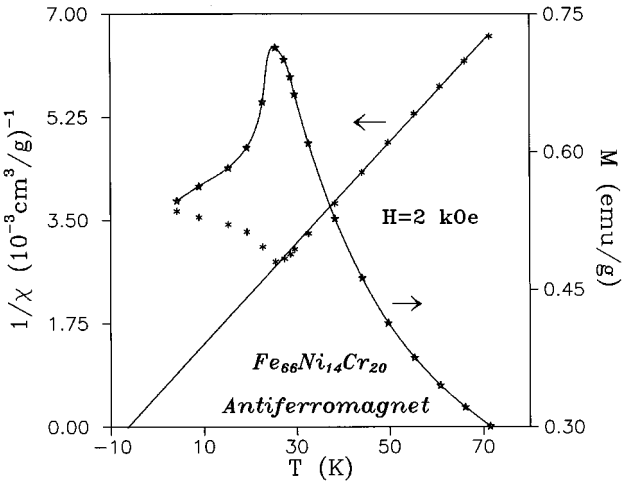

FIG. 8. Reciprocal susceptibility ($1/\chi$) and magnetization (M) vs temperature (T) for $Fe_{66}Ni_{14}Cr_{20}$ alloy at 0.2 T. Θ is small but negative and the Néel temperature is (26 ± 1) K.

TABLE III. Composition (x), Curie constant (C), effective Bohr magneton number (P_{eff}), paramagnetic Curie temperature (Θ), q_c, q_s, temperature for the onset of deviation from Curie-Weiss law (T_d), and effective number of electrons per atom outside the closed argon shell [$n(\approx\langle 3d+4s\rangle$)], of $Fe_{80-x}Ni_xCr_{20}$ alloys.

x (Ni conc.)	C (10^{-3} cm^3 K/g)	P_{eff} (μ_B)	Θ (K)	q_c (μ_B)	q_s (μ_B)	T_d (K)	$n\simeq\langle 3d+4s\rangle$
14	11.7	2.28	–6.5	1.49		26	7.88
19	8.7	1.97	43	1.20		98	7.98
21	12.1	2.31	50	1.52		130	8.02
23	13.2	2.42	127	1.62	0.13	280	8.06
26	15.7	2.65	100	1.83	0.27	300	8.12
30	13.0	2.42	190	1.61	0.40	320	8.20

There is a subtle interplay between the effective number $n(\approx\langle 3d+4s\rangle)$ of electrons per atom outside the closed argon shell and the type of magnetic ordering as well as their transition temperatures. In Table III we give the values of n for all the alloys. For $n>8$, these alloys shift towards the FM state with increasing spontaneous moment (M_0) and T_c. On the other hand, when $n<8$, AFM ordering is established, while in the intermediate region the SG phase appears.

The above facts, namely, the nonintegral values of $\overline{\mu}$ in Bohr magneton per atom, the strong deviation from Slater-Pauling curve, the curvature in the low-field region, and a set of parallel lines in the high-field region of the ABK plots, the large values of χ_{HF} at 19 T and 4.2 K, and the Mathon plots, indicate the possibility that the alloys with higher Ni concentration having FM ordering at lowest temperatures may be described within the framework of the itinerant model rather than the localized one. We have examined the FM ordering in the light of the Rhodes-Wohlfarth[54] criteria: (a) In the localized model the effective spin is the actual spin and hence $q_c/q_s=1$, for all T_c, where $P_{eff}=\sqrt{q_c(q_c+2)}$ in the PM state and q_s is the average spontaneous moments in the units of μ_B and (b) in the itinerant model q_s might be less than the maximum possible value q_c, and hence $q_c/q_s>1$ and its value (between 1 and ∞) gives a measure of the degree of itinerancy. In addition, $q_c/q_s\propto T_c^{-1}$ for itinerant electrons; i.e., the larger the ratio (q_c/q_s), the weaker is the FM. The values of q_c and q_s are given in Table III for the alloys with $x=30$, 26, and 23. It is quite apparent that q_c/q_s indeed shows a systematic increase with decreasing T_c and follows the relation $q_c/q_s\propto T_c^{-1}$. Moreover, q_c/q_s lies between 4 and 12, indicating moderate itinerancy. They also compare favorably with those of several other weak itinerant FM alloys [e.g., FeCr, FeV, NiFeV (Ref. 55), ZrZn (Ref. 56).] Thus we conclude that the alloys with higher x (23–30) are weak itinerant ferromagnets (WIF's).

B. Spin-wave analysis of γ-$Fe_{50}Ni_{30}Cr_{20}$ alloy

There are reports on Fe-Ni-based crystalline and amorphous alloys (e.g., $Fe_xNi_{80-x}B_{18}Si_2$,[57] Ni-Fe-Cr, Ni-Fe-V,[55] etc.) where the presence of both spin-wave and Stoner single-particle excitations was confirmed through bulk magnetization measurements. Inelastic neutron scattering[37] studies directly prove the presence of spin-wave excitations in these alloys. It was concluded for Ni-rich Ni-Fe-Cr and Ni-Fe-V alloys[55] that the addition of Cr and V enhances the Stoner term considerably, and drives these systems towards the weak itinerant FM regime.

To examine contributions from various kinds of excitations to the temperature-dependent demagnetization process, we have carried out very careful dc-magnetization $M(T)$ measurements (accuracy 1 part in 10^4) at a 100-mK temperature interval in a field of 1 T. In Fig. 9, we show the $M(T)$ data which have been analyzed in the light of the spin-wave (SW) theory as well as Stoner excitations.[58–60] At low temperatures, the change in magnetization due to spin-wave excitations is given by

$$\left[\frac{\Delta M(T)}{M(0)}\right]_{SW}=\frac{M(T)-M(0)}{M(0)}$$
$$=AT^{3/2}(1-D_1T^2-D_2T^{5/2})^{-3/2}$$
$$\times\mathcal{Z}(3/2,T_g/T)+BT^{5/2}\mathcal{Z}(5/2,T_g/T). \quad (5)$$

Here T_g is the gap temperature which is equal to $g\mu_BH_{int}/k_B$, $\mathcal{Z}(3/2,T_g/T)$ and $\mathcal{Z}(5/2,T_g/T)$ are the Bose-

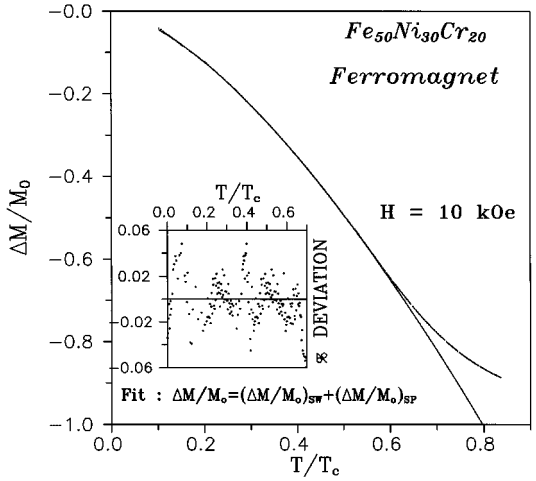

FIG. 9. Change of reduced magnetization ($\Delta M/M_0$) as a function of reduced temperature (T/T_c) for $Fe_{50}Ni_{30}Cr_{20}$ (FM) alloy. The solid line is the nonlinear least-squares fit of the experimental data to the combination of *spin-wave* and Stoner *single-particle* excitations. The percentage deviation of the fit from the data, shown in the inset, implies a very good quality of fit.

Einstein integrals, and the coefficient A is related to the spin-wave stiffness constant $\mathcal{D}(0)$, by

$$\mathcal{D}(0)=\frac{k_B}{4\pi}\left(\frac{2.612g\mu_B}{M(0)\rho A}\right)^{2/3}, \tag{6}$$

where ρ is the density. Thompson *et al.*[61] have calculated the change in reduced magnetization due to Stoner single-particle (SP) excitations only, given by

$$\left[\frac{\Delta M}{M(0)}\right]_{\mathrm{SP}}=\alpha T^{3/2}e^{-\Delta/k_BT} \tag{7}$$

for strong itinerant FM and

$$\left[\frac{\Delta M}{M(0)}\right]_{\mathrm{SP}}=\beta T^2, \tag{8}$$

for weak itinerant FM. Here α and β are related to various band parameters. Δ is the energy gap between the top of the full subband and the Fermi level (E_F) for a strong FM. It is 0 for a weak FM.

At low temperatures, when deviation from saturation magnetization at 0 K is small, the excitations from the SW and the SP are nearly independent and the thermal demagnetization is given by the sum of both the contributions, i.e.,

$$\Delta M=[\Delta M]_{\mathrm{SW}}+[\Delta M]_{\mathrm{SP}}. \tag{9}$$

We used a nonlinear least-squares fitting program using the NAG library to fit the $M(T)$ data for the alloy with $x=30$. The fit to Eq. (5) excluding the $BT^{5/2}$ anharmonic term gives $\chi^2=6.8\times10^{-6}$ which is at least one order of magnitude higher than the experimental error. Inclusion of the anharmonic term yields an unphysical sign of the coefficient B. However, the data, when fitted to Eq. (9), a combination of Eqs. (5) and (8) but excluding the anharmonic $T^{5/2}$ term, yield a much improved $\chi^2=2.1\times10^{-7}$ with $A=3.4\times10^{-4}$ K$^{-3/2}$ and $\beta=9.3\times10^{-7}$ K^{-2}. As shown in Fig. 9, the experimental data and the best-fitted curves are almost indistinguishable. But Eq. (9), when taken as a combination of Eqs. (5) and (7), gives unphysical values of α and the gap parameter Δ. In the inset of Fig. 9 we have also shown the percentage deviation of the fit from the data which clearly reveals that a combination of both SW and SP excitations describes the thermal demagnetization process quite well in this FM alloy. The value of the coefficient of the SW term $A(\approx10^{-4}$ K$^{-3/2})$ is two orders of magnitude larger than those of pure Fe and Ni ($\approx10^{-6}$ K$^{-3/2}$) (Ref. 59) and one order of magnitude larger than those of Ni-rich Ni-Fe-Cr and Ni-Fe-V alloys ($\approx10^{-5}$ K$^{-3/2}$) (Ref. 55). This implies that the spontaneous magnetization (M_0) of the alloy falls off with temperature at a faster rate and so it must have a weaker SW stiffness constant $\mathcal{D}(0)$. Using Eq. (6) we have estimated $\mathcal{D}(0)$ to be ≈40 meV Å^2 whereas it is 286, 100, and 46 meV Å^2 for pure Fe,[59] Ni-rich $Ni_{67}Fe_{21}Cr_{12}$,[55] and higher Cr-containing amorphous alloys like $Fe_5Co_{50}Ni_2Cr_{15}B_{16}Si_{12}$,[42] respectively. It should be noted that with the addition of Cr in Ni-Fe binary alloys, $\mathcal{D}(0)$ falls off very rapidly.[55,42] Moreover, as far as the magnetic properties are concerned, there is not much difference between the crystalline and amorphous materials. Our estimated value of $\mathcal{D}(0)$ for the alloy with $x=30$ seems rather reasonable. In addition to this there is also a strong experimental support to our result from the inelastic neutron scattering studies by Men'shikov *et al.*[37] on Ni-rich Ni-Fe-Cr alloys from which the SW stiffness constant $\mathcal{D}(0)$ was estimated to be ≈50 meV Å^2. They also could not detect the presence of any higher-order term apart from the quadratic one in the SW dispersion relation, in good agreement with our result. Thus we conclude that the introduction of Cr suppresses the anharmonic term ($T^{5/2}$), similar to the earlier case.[55] Moreover, the Stoner single-particle excitation is present in this weak itinerant FM. The constant β in the Stoner term is of the same order as in pure Ni (Ref. 59) and Ni-rich Ni-Fe-Cr (Ref. 55) alloys ($\approx10^{-7}$ K^{-2}). Thus one finds that the addition of Cr enhances the Stoner term considerably.

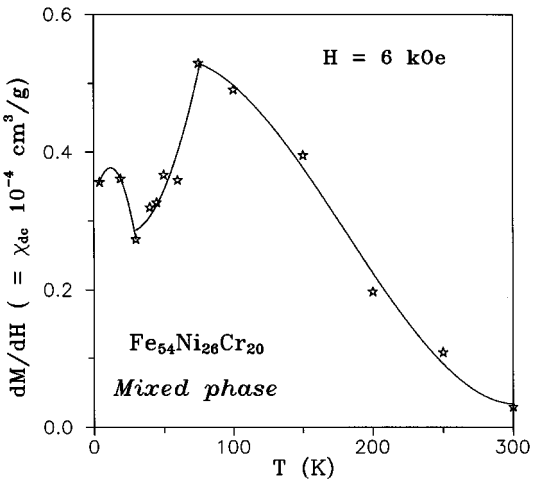

FIG. 10. Temperature dependence of dc susceptibility χ_{dc} ($=dM/dH$) for the mixed phase alloy $Fe_{54}Ni_{26}Cr_{20}$ at a field of 0.6 T. The solid line is a guide to the eye. The peaks appear at the respective transition temperatures (T_c and T_f).

C. $x=26$: Mixed-phase alloy

In Fig. 10 the temperature dependence of the dc susceptibility χ_{dc} ($=dM/dH$) is shown in a field of 0.6 T which is above the technical saturation for the alloy with $x=26$. We find that there is a sharp peak in χ_{dc} at around $T\approx60$ K which is the PM→FM transition temperature (T_c) as reported earlier.[30] As the temperature decreases, χ_{dc} decreases continuously. But below some minimum temperature it again starts to increase significantly. In our earlier work[38] we made the same kind of observation for the alloy with $x=23$ and 21 which have mixed phase and SG orderings, respectively, at the lowest temperature. Hamzic and Campbell[62] also made exactly the same kind of observation for the variation of χ_{dc} with temperature in the case of Au 19% Fe alloy which is beyond the percolation threshold where long-range FM appears alongwith SG freezing. In this alloy with $x=26$, there is a coexistence between FM and SG orderings at the lowest temperature. So this is a common feature of χ_{dc} which is observed in a number of alloys having either SG or mixed phase orderings.

The alloy with $x=26$, below a temperature $T_f=7$ K, has a SG ordering as reported in different investigations.[30] There is

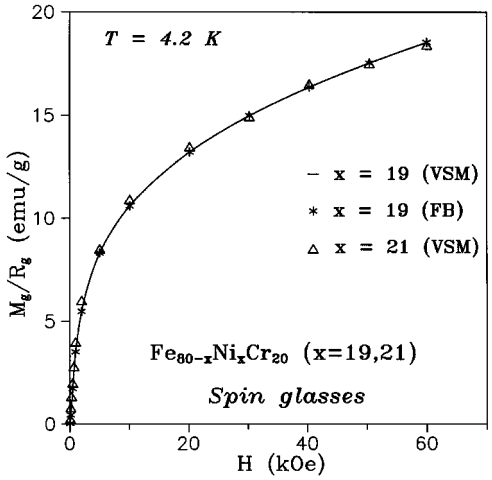

FIG. 11. M-H plot of the alloy with $x=21$ is scaled onto that of $x=19$, implying the same kind of magnetization process at 4.2 K. The abbreviations VSM and FB stand for vibrating sample magnetometer and Faraday balance, respectively.

a long-standing controversy for this kind of mixed phase or reentrant phase alloys[63] showing double transitions. Whether both kinds of ordering, namely, SG and FM, coexist below the second transition is still debatable. From a number of experimental evidence[15,17,20,64,65] it was concluded that both orderings do coexist below the second transition. This kind of behavior can be understood through the *semi-spin-glass* picture proposed by Villain.[13] Just below T_c these alloys behave as a standard FM with (for each spin) $m_z^i \neq 0$, $m_x^i = m_y^i = 0$. As the temperature drops, the degree of FM ordering increases continuously and hence $\chi_{\rm dc}$ drops below T_c. But at a lower temperature the spins begin to acquire random uncorrelated canted moment with components m_x^i, $m_y^i \neq 0$ but $\langle m_x \rangle = \langle m_y \rangle = 0$. At the lowest temperature (below the second transition) the conventional spin-wave theory totally breaks down. This has been clarified later by the Gabay-Toulouse (GT) model, which is a Heisenberg version of the Sherington-Kirkpatrick model, where below the second transition temperature there is an overall long-range order in a certain direction (say, the z direction) and a simultaneous existence of frozen spins in the transverse direction (x-y plane). So the temperature dependence of $\chi_{\rm dc}$ of this mixed phase alloy can be understood in the light of the Villain as well as the GT models. We have also seen from Arrott plots (Fig. 5) that at the lowest temperature (4.2 K), FM ordering persists in this alloy. Moreover, thermoremanent-history-dependent FC magnetization[30] confirmed the SG ordering at 4.2 K. So our results for $\chi_{\rm dc}$ as well as the Arrott plots definitely support the coexistence of both FM and SG orderings below the second transition.

D. $x=19$ and 21: Spin-glass alloys

A remarkable feature of the magnetization curves for the alloys with $x = 19$ and 21 is that the curves can be scaled on a single universal curve until very high fields as shown in Fig. 11. Both the alloys have only one transition (PM→SG) at 12 and 10 K, respectively.[30] The magnetization curve for the higher-concentration alloy ($x=21$) can be brought into coincidence with that of $x=19$ by using a scaling factor defined as $R_g = M(x)/M(x=19)$. The magnetization data for $x=21$,[30] obtained by using the Faraday balance (FB) technique, are also brought into coincidence on the same figure with the same scaling factor, i.e., irrespective of the measurement technique. The universality of the behavior of the magnetization implies the same magnetization process, namely, the high-field response dynamics of the frozen spins. This kind of universal scaled magnetization curve was also observed in archetypical SG [CuMn and AuFe (Refs. 66 and 46)] systems below the critical concentration. For the alloys with $x=26$, 23, and 14, the scaled magnetization curves have strong deviations from a universal one, suggesting entirely different kinds of magnetization processes.

E. $x=14$: Antiferromagnetic alloy

As mentioned earlier, the $M(H)$ curve at 4.2 K has an inflection point at around 1 T as shown in Fig. 3 with an arrow. The figure also shows a dM/dH vs H plot which has a sharp peak at the inflection point at the same field. We have further observed that the point of inflection shifts slightly towards low fields at higher temperatures of 11.2 and 20.1 K. The $M(H)$ curves (at T=35.1 and 60 K) beyond the Néel temperature ($T_N=26$ K) do not show any inflection point. The field $H_c = 1$ T can be taken as the critical field for the *spin-flop* transition below T_N. This alloy has a long-range AFM ordering with a reasonably small value of the Néel temperature ($T_N=26$ K). A number of reports show that *spin flopping* can be produced most easily if the Néel temperature is low and for them H_c will be relatively small (e.g., $CuCl_2 \cdot 2H_20$ ($T_N=4.2$ K),[67] MnF_2, Cr_2O_3, DyAg,[68] DyAu,[68] Au_3Mn, etc.).

Unlike the conventional AFM's, this alloy shows a high value of the field-induced moment at 19 T ($\approx 0.17 \mu_B$) and a tendency of saturation (Fig. 1). Neutron scattering in AFM γ-$Fe_{0.7}Ni_{0.15}Cr_{0.15}$ (Ref. 33) in magnetic fields of 5 T suggested that the induced moment can be interpreted in terms of the canting of the AFM spins. In the alloy with $x=14$, the magnetization M induced in the high magnetic field H obeys the Landau relation of the form

$$M^2 = -A + BH/M, \tag{10}$$

with $A=308$ (emu/g)^2 and $B=560$ (emu/g)^3/T in the field range between 10 and 20 T at 4.2 K. This relation holds when the substance is close to a FM state but as a whole is an AFM. However, there may exist a positive interaction between the high-field-induced moments as had been concluded in the AFM γ-$Fe_{0.7}Ni_{0.15}Cr_{0.15}$ (Refs. 32 and 33) alloy. An itinerant AFM model[32] was proposed in which the effective magnetic interaction between the spins is always positive even in an AFM substance, and an AFM state can also be close to a FM state. The effect of magnetic field on the AFM structure was studied by neutron scattering measurements[33] on γ-$Fe_{0.7}Ni_{0.15}Cr_{0.15}$. It suggested that the induced moment could be explained by canting of the AFM spins by an angle θ.

We have used the experimentally estimated parameters T_N ($\simeq 26$ K), C ($\simeq 11.7 \times 10^{-3}$ cm^3 K /g), and the paramagnetic Néel temperature Θ ($\simeq -6.4$ K) (some are shown in

Table III) to evaluate J_1, J_2, γ_1, and γ_2 for this alloy with $x=14$. Here J_i is the effective-field exchange interaction between the ith neighbors. Similarly, γ_1 and γ_2 are the first- and second-neighbor molecular field coefficients. In the light of Smart's model[69] for the generalized molecular field theory for an antiferromagnetic substance with n sublattices, the following relations can be written:

$$\gamma_{ij}=\frac{2nZ_{ij}J_{ij}}{Ng^2\mu_B^2}, \quad i\neq j, \tag{11}$$

$$\Theta=\frac{C}{n}\sum_{j=1}^{n}\gamma_{ij}, \tag{12}$$

and

$$T_{N_s}=\frac{C}{n}\sum_{j=1}^{n}\eta_{ij}J_{ij}, \tag{13}$$

where Z_{ij} is the number of j neighbors of an i atom, J_{ij} the exchange interaction between an i atom and one of its j neighbors, γ_{ij} the molecular field coefficient for the field exerted on an atom on the ith sublattice by its neighbors on the jth sublattice, and μ_B the Bohr magneton. The present AFM alloy has a fcc structure. According to Smart,[69] an AFM alloy with fcc structure can have a maximum of possible three types of antiferromagnetic ordering. Our calculation for the alloy with $x=14$ is appropriate for the fcc structure with *type 1* antiferromagnetic ordering with 8 sublattices and 12 nearest- as well as 6 next-nearest-neighbor atoms.[69] Using Eqs. (11)–(13) we have computed the following values: $\gamma_1=-20.8\times10^5$ kg/m^3, $\gamma_2=15.3\times10^5$ kg/m^3, $J_1/k=-1.29$ K, and $J_2/J_1=-1.47$. In this AFM alloy, Θ/T_N ($\simeq-0.25$) is small and negative, in contrast with the large values (>1) observed in the SG alloys ($x=19$ and 21, Table III). This indicates that frustration effects are minimal in this alloy with $x=14$. From the above estimates, a number of important inferences could be drawn, e.g., negative values of J_1 and J_2/J_1 indicate that the first nearest-neighbor interaction is AFM and the second nearest-neighbor interaction is FM. $|J_2/J_1|>1$ implies that the second nearest-neighbor interaction is stronger than the first. The larger value of J_2 compared to J_1 does not affect the effective-field approximation used here, because there are 12 nearest neighbors, each contributing $-|J_1|$ towards Θ, whereas there are only 6 next-nearest neighbors, each with a contribution of $\approx1.5J_1$. Hence as a whole the paramagnetic Néel temperature Θ is still negative (antiferromagnetic) and has a small value as observed experimentally. Because of the fact that $|J_2/J_1|>1$, one concludes that this alloy must have a strong itinerant-electron contribution. Perhaps some of the outer $3d$ and $4s$ electrons are localized and some others are in the extended states. The nearest-neighbor molecular-field coefficient $\gamma_1<0$ implies the expected AFM interaction. The next-nearest-neighbor interaction $\gamma_2>0$ corresponds to the FM interaction. The values of Θ/T_N and γ_2/γ_1 are compatible only with the *type 1* AFM ordering in this alloy. All these results agree with neutron-diffraction-derived structural studies[32,33] which revealed the *type 1* AFM ordering in alloys of a similar composition.

IV. CONCLUSION

In this work we have carried out systematic high-field (0–20 T) dc-magnetization studies [$M(H)$ and $M(T)$ between 4.2–60 K and 19–700 K, respectively] on substitutionally disordered γ-$Fe_{80-x}Ni_xCr_{20}$ ($14\leqslant x\leqslant 30$), austenitic stainless steel alloys having a very rich magnetic phase diagram at low temperatures. We find a number of distinct functional relationships $M(H)$ in different magnetic phases below their respective magnetic transition temperatures. Because of the very large χ_{HF} compared to that of a conventional FM, we conclude that the nature of ferromagnetism in the case of the alloys with $x=30$, 26, and 23 in their FM phase is unlike that of a standard FM. They are very hard to saturate even at a field of 19 T at 4.2 K. The law of approach to saturation reproduces the high-field $M(H)$ data in the saturation regime reasonably well. In the light of the *Rhodes-Wohlfarth* criterion the alloys with $x=30$, 26, and 23 in their FM regime are of weak itinerant type. In the FM alloy with $x=30$, the combination of long-wavelength *spin-wave* and *Stoner single-particle* excitations describes the thermal demagnetization process quite well until $0.5T_c$. We conclude that the introduction of Cr in this alloy substantially reduces the *spin-wave stiffness constant* $\mathcal{D}(0)$, suppresses the anharmonic term ($T^{5/2}$), and enhances the Stoner term.

In the case of the alloys with $x=26$ and 23 (mixed phase), this particular study, along with our earlier studies, corroborates that below the second transition long-range FM ordering coexists with transverse SG freezing, supporting the GT model. Neutron-depolarization studies coupled with small-angle neutron scattering would be able to provide a complete picture of the transverse spin component in the FM domain (which might be of vortexlike spin structure), the nature of the domain-wall motion, and the spin-modulated structure. In the concentrated SG alloys ($x=21$ and 19) the high-field response dynamics of the frozen spins is similar to that of the *archtypical* spin glasses.

Our analysis of the $x=14$ (AFM) alloy shows that the long-range AFM structure of this alloy is of *type 1* where the first nearest-neighbor interaction (J_1) is AFM and the second one is FM (J_2). Since $|J_2/J_1|>1$, we conclude that this alloy must have a strong itinerant-electron-AFM contribution. It also shows a *spin-flop* transition at 1 T due to the canting of the AFM spins in the strong external magnetic field. Beyond this transition a square-root dependence of magnetization with external field is found whereas below it the dependence is linear.

At present as there is no band structure (electronic or magnetic) calculation in these alloys, it is very difficult to estimate and correlate anything in more quantitative terms. Greater attention must be paid in this direction for better correlation of the transport and magnetic properties of these ternary alloys.

ACKNOWLEDGMENTS

N.S. thanks Thomas Ankermann of Process Systems International, Inc., for sponsoring some of the experiments at FBNML and the warm hospitality extended during his visit. Financial assistance from Project No. SP/S2/M-24/93 of the Department of Science and Technology, Government of India, is gratefully acknowledged.

[1] V. Korenman, J. Murray, and R. E. Prange, Phys. Rev. B **16**, 4032 (1977).
[2] T. Moriya and Y. Takahashi, J. Phys. Soc. Jpn. **45**, 397 (1978); J. Phys. (Paris) Colloq. **39**, C6-1466 (1978).
[3] Yoshiro Kakehashi, J. Magn. Magn. Mater. **37**, 189 (1983); Y. Kakehashi and O. Hosohata, Phys. Rev. B **40**, 9080 (1989) and references therein.
[4] R. Dreizler and E. Gross, *Density Functional Theory* (Springer-Verlag, New York, 1990); S. Peng and H. Jansen, Phys. Rev. B **43**, 3518 (1991); P. Ordejon, D. Drabold, M. Grambach, and R. Martin, *ibid.* **51**, 1456 (1995).
[5] Henri J. F. Jansen, Phys. Today **48** (4), 50 (1995).
[6] R. Bozorth, *Ferromagnetism* (Van Nostrand-Reinhold, Princeton, 1951), p. 441.
[7] J. Friedel, Can. J. Phys. **34**, 1190 (1956); Nuovo Cimento Suppl. **7**, 287 (1958).
[8] G. G. Low and M. F. Collins, J. Appl. Phys. **34**, 1195 (1963); G. G. Low, *ibid.* **39**, 1174 (1968); M. F. Collins and G. G. Low, Proc. Phys. Soc. London **86**, 535 (1965).
[9] H. Bouchiat, J. Phys. C **16**, L145 (1983); **30**, 3963 (1984); A. P. Malozemoff, S. E. Barnes, and B. Barbara, Phys. Rev. Lett. **51**, 1704 (1983).
[10] J. Gelard, F. Bensamka, D. Bertand, A. R. Fert, J. P. Redoules, and S. Legrand, J. Phys. C **16**, L939 (1983).
[11] A. Banerjee and A. K. Majumdar, Phys. Rev. B **46**, 8958 (1992).
[12] M. Gabay and G. Toulouse, Phys. Rev. Lett. **47**, 201 (1981).
[13] J. Villain, Z. Phys. **33**, 31 (1979).
[14] K. Binder and A. P. Young, Rev. Mod. Phys. **58**, 801 (1986).
[15] B. R. Coles, B. Sarkissian, and R. H. Taylor, Philos. Mag. B **37**, 489 (1978); B. V. B. Sarkissian, J. Phys. F **11**, 2191 (1981).
[16] J. Hesse, Ch. Böttger, A. Wulfes, J. Sievert, and H. Ahlers, Phys. Status Solidi A **135**, 343 (1993).
[17] H. Kunkel, R. M. Roshko, W. Ruan, and G. Williams, Philos. Mag. B **64**, 153 (1991).
[18] I. A. Campbell, H. Hurdequint, and F. Hippert, Phys. Rev. B **33**, 3540 (1986); I. A. Cambell, S. Senoussi, F. Varret, J. Teillet, and A. Hamzic, Phys. Rev. Lett. **50**, 1615 (1983).
[19] S. Senoussi, S. Hadjoudj, and R. Fourmeaux, Phys. Rev. Lett. **61**, 1013 (1988); S. Hadjoudj, S. Senoussi, and I. Mirebeau, J. Magn. Magn. Mater. **93**, 136 (1991).
[20] W. Abdul-Razzaq and J. S. Kouvel, Phys. Rev. B **35**, 1764 (1987); J. S. Kouvel and W. Abdul-Razzaq, J. Magn. Magn. Mater. **53**, 139 (1985).
[21] I. Mirebeau, S. Itoh, S. Mitsuda, F. Watanabe, Y. Endoh, M. Hennion, and P. Calmettes, J. Appl. Phys. **67**, 5232 (1990).
[22] T. Sato, T. Ando, T. Watanabe, S. Itoh, Y. Endoh, and M. Furusaka, Phys. Rev. B **48**, 6074 (1993).
[23] B. Huck and J. Hesse, J. Magn. Magn. Mater. **78**, 247 (1989).
[24] Jürgen Hesse, Hyperfine Interact. **47**, 357 (1989).
[25] B. H. Verbeek, G. J. Nieuwenhuys, H. Stocker, and J. A. Mydosh, Phys. Rev. Lett. **40**, 586 (1978).
[26] S. B. Roy and B. R. Coles, J. Phys. Condens. Matter. **1**, 419 (1989).
[27] S. J. Kennedy and B. R. Coles, J. Phys. Condens Matter. **2**, 1213 (1989).
[28] S. B. Roy and B. R. Coles, Philos. Mag. B **54**, 741 (1991).
[29] T. Moriya and K. Usami, Solid State Commun. **23**, 935 (1977).
[30] A. K. Majumdar and P. v. Blanckenhagen, Phys. Rev. B **29**, 4079 (1984).
[31] A. Z. Men'shikov and A. Ye. Teplykh, Fiz. Metal. Metalloved. **44**, 1215 (1977).
[32] Y. Ishikawa, Y. Endoh, and T. Takimoto, J. Phys. Chem. Solids **31**, 1225 (1970).
[33] Y. Ishika, M. Kohgi, and Y. Noda, J. Phys. Soc. Jpn. **39**, 675 (1974).
[34] F. Gautier, in *Magnetism of Metals and Alloys*, edited by M. Cyrot (North-Holland, New York, 1982), p. 1; F. J. Pinski, J. Stanton, B. L. Gyroffy, D. D. Johnson, and G. M. Stocks, Phys. Rev. Lett. **56**, 2096 (1986).
[35] Sidney H. Avnar, *Introduction to Physical Metallurgy* (McGraw-Hill, New York, 1987).
[36] A. K. Majumdar and P. v. Blanckenhagen, J. Magn. Magn. Mater. **40**, 227 (1983).
[37] A. Z. Men'shikov, N. N. Kuz'min, V. A. Kazantsev, S. K. Sidorov, and V. N. Kalinin, Phys. Metal. Metalloved. **40**, 174 (1975).
[38] T. K. Nath and A. K. Majumdar, J. Appl. Phys. **70**, 5828 (1991).
[39] T. K. Nath and A. K. Majumdar, Phys. Rev. B **53**, 12 148 (1996).
[40] S. Banerjee and A. K. Raychaudhuri, Phys. Rev. B **50**, 8195 (1995).
[41] Lawrence G. Rubin and Peter A. Wolf, Phys. Today **37** (8), 24 (1984).
[42] A. Das and A. K. Majumdar, J. Magn. Magn. Mater. **128**, 47 (1993).
[43] T. Sakakibara, T. Goto, and Y. Miyako, Solid State Commun. **58**, 563 (1986).
[44] H. Hiroyoshi and K. Fukamichi, J. Appl. Phys. **53**, 2226 (1982); S. N. Kaul, Phys. Rev. B **27**, 6923 (1983); H. Hiroyoshi, N. Saito, K. Fukamichi, and Y. Nakagawa, Sci. Rep. Res. Inst. Tohoku Univ. A **33**, 58 (1986).
[45] G. Toulouse, J. Phys. (Paris) Lett. **41**, L447 (1980).
[46] J. J. Smit, G. J. Nieuwenhuys, and L. J. de Jongh, Solid State Commun. **32**, 233 (1979).
[47] H. Hiroyoshi, K. Fukamichi, A. Hoshi, and Y. Nakagawa, in *High Field Magnetism*, edited by M. Date (North-Holland, Amsterdam, 1983), p. 113.
[48] J. Schneider, Physica **91B**, 185 (1977); J. Phys. C **8**, 682 (1980); J. Schneider, A. Handstein, and K. Zaveta, J. Magn. Magn. Mater. **42**, 73 (1984).
[49] S. Shtrikman and E. P. Wohlfarth, Physica **60**, 427 (1972).
[50] D. M. Edwards and E. P. Wohlfarth, Proc. R. Soc. London, Ser. A **303**, 127 (1968).
[51] R. D. Shull and P. A. Beck, in *Magnetism and Magnetic Materials*, edited by C. D. Graham, G. H. Lander, and J. J. Rhyne, AIP Conf. Proc. No. 24 (AIP, New York, 1975), p. 95.
[52] V. I. Pecherskaya, D. N. Bol'shutkin, A. V. Butenko, V. N. Beilinson, V. I. Ovcharenko, V. A. Pervakov, and N. Yu. Tyutryumova, Sov. J. Low Temp. Phys. **14**, 505 (1988).
[53] J. Mathon, Proc. R. Soc. London, Ser. A **306**, 355 (1968); J. Mathon and E. P. Wohlfarth, Phys. Status Solidi **30**, K 131 (1968).
[54] P. Rhodes and E. P. Wohlfarth, Proc. R. Soc. London, Ser. A **273**, 247 (1963); E. P. Wohlfarth, J. Magn. Magn. Mater. **7**, 113 (1978).
[55] A. K. Gangopadhyay, R. K. Ray, and A. K. Majumdar, Phys. Rev. B **30**, 6693 (1984).
[56] D. A. Reed, E. H. Thomas, and J. B. Forsythe, J. Phys. Chem. Solids **29**, 1569 (1968); G. S. Knapp, F. Y. Fradin, and H. V. Culbert, J. Appl. Phys. **42**, 1341 (1971).
[57] E. Babic, Z. Marohnic, and E. P. Wohlfarth, Phys. Lett. **95A**, 335 (1983).

[58] F. Keffer, in *Handbuch der Physik*, edited by S. Flügge (Springer, Berlin, 1966), Vol. XVIII/2.

[59] B. E. Argyle, S. H. Charap, and E. W. Pugh, Phys. Rev. **132**, 2051 (1963).

[60] C. Herring, in *Magnetism*, edited by G. T. Rado and H. Suhl (Academic Press, New York, 1966), Vol. IV; W. Marshall and S. W. Lovesey, *Theory of Thermal Neutron Scattering* (Oxford, University Press, New York, 1971).

[61] E. D. Thompson, E. P. Wohlfarth, and A. C. Bryan, Proc. Phys. Soc. London **83**, 59 (1964).

[62] A. Hamzic and I. A. Campbell, J. Phys. (Paris) Lett. **42**, L-309 (1981).

[63] G. Aeppli, S. M. Shapiro, H. Maletta, R. J. Birgeneau, and H. S. Chen, J. Appl. Phys. **55**, 1628 (1984), and references therein.

[64] M. Avirovic, P. Ziemann, B. Huck, and J. Hesse, Europhys. Lett. **8**, 281 (1989).

[65] B. H. Verbeek, G. J. Nieuwenhuys, H. Stocker, and J. A. Mydosh, Phys. Rev. Lett. **40**, 586 (1978).

[66] J. J. Smit, G. J. Nieuwenhuys, and L. J. de Jongh, Solid State Commun. **31**, 265 (1979).

[67] N. J. Poulis, J. van den Handel, J. Ubbink, J. A. Poulis, and C. J. Gorter, Phys. Rev. **82**, 552 (1951); C. J. Gorter, Rev. Mod. Phys. **25**, 277 (1953).

[68] T. Kaneko, Shunya Abe, H. Yamauchi, H. Hiroyoshi, and Akira Hoshi, in *High Field Magnetism*, edited by M. Date (North-Holland, Amsterdam, 1983), p. 108.

[69] J. S. Smart, *Effective Field Theories of Magnetism* (Saunders, Philadelphia, 1966).